Electronic Supplementary Information

Gum Arabic induced assembly of Cellulose Nanocrystals in aqueous media

David Attia[1], Yael Levi-Kalisman[2], Ronit Bitton[1,3], and Rachel Yerushalmi – Rozen[1,3*]

[1] Department of Chemical Engineering, Ben-Gurion University of the Negev, Beer Sheva 84105, Israel.

[2] The Center for Nanoscience and Nanotechnology, The Hebrew University, Jerusalem 91904, Israel.

[3] The Ilse Katz Institute for Nanoscience and Technology, Ben-Gurion University of the Negev, Beer-Sheva 84105, Israel.

* Corresponding author at: Department of Chemical Engineering and The Ilse Katz Institute for Nanoscience and Technology, Ben-Gurion University of the Negev, Beer Sheva 84105, Israel. E-mail address: rachely@bgu.ac.il (R. Yerushalmi-Rozen).

1. Introduction

The effect of non-adsorbing polymers on the kinetics, self-assembly and gelation of Cellulose nanocrystals (SCNCs) in aqueous suspensions was investigated by a few groups. Edgar and Gray [1] found that Dextran did not modify the phase diagram of CNCs, but preferentially partitioned into the isotropic phase. The effect of polyethylene glycol (PEG) on the kinetics of self-assembly was investigated by Sun *et al*.[2] They reported modification of the kinetics in low Mw. PEG (20 kDa), and gelation leading to the formation of a nematic (rather than cholesteric) phase in solutions of high Mw. PEG (200 kDa). The effect of anionic (carboxymethyl cellulose CMC) on the physical behavior of SCNCs was investigated by Oguzlu et al.[3,4] The authors reported depletion induced flocculation of SCNCs into gel-like structures in solutions of (non-adsorbing) Carboxymethyl cellulose followed by macroscopic phase separation, where the isotropic phase is enriched by the polymer. Bardet et al.[5] investigated the effect of anionic (sodium polyacrylate) cationic (polyethylenimine) and neutral (polyethylene glycol), water-soluble polymers, on the self-assembly of SCNC. They found that PEG does not lead to flocculation of the suspended CNCs. They briefly described the absence of a significant effect by the non-adsorbing sodium polyacrylate and attributed the observations to depletion effect.

2. Results

2.1. Small-angle X-ray scattering (SAXS) of GA solutions

The structure of solvated GA was investigated using SAXS, at room temperature. 1D SAXS curves of 1-5 wt% GA solutions are presented in Figure S1. The scattering pattern is characterized by a well-defined peak. The position and shape of the peak depend on the concentration of GA. As the concentration increases, the peak shifts to higher values of q and broadens. The scattering patterns were fitted to the broad Lorentzian peak empirical model:[6]

$$I(q) = \frac{A}{q^n} + \frac{C}{1 + \left(|q - q_0|\xi\right)^m} \quad \text{(S1)}$$

Where A is the Porod law scale factor, n is the Porod exponent, here n = 0, and A = 0. C is the Lorentzian scale factor, q_0 is the peak maximum, ζ is the correlation length, and m is roughly equal to $1/\nu$, where ν is the Flory exponent, which indicates the behavior of a polymer in a solvent (3/5 for good solvent, 1/2 for theta solvent).

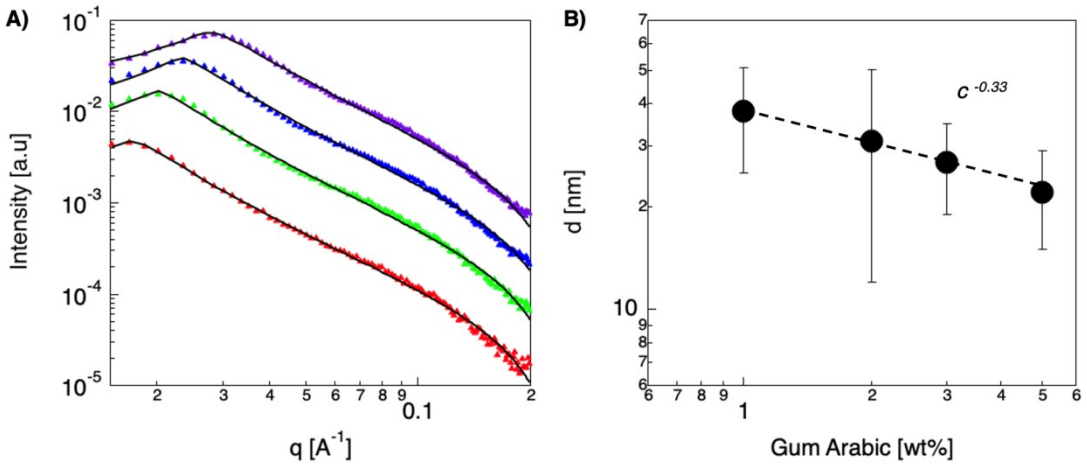

Figure S1. A) 1D SAXS patterns obtained from GA solutions at different concentrations (1 wt% ▲, 2 wt% ▲, 3 wt% ▲, 5 wt% ▲). The solid lines represent a fit to the broad peak model.[32] The curves are shifted for better visualization. **B)** The inter-aggregate distance *d*, as calculated from SAXS measurements, as a function of GA concentration.

The scattering patterns indicate an inter-aggregate distance *d* that decreases with concentration as $d \sim c^{-1/3}$, as expected for a dilute solution of charged polyelectrolytes. [7] [8] The best-fit parameters are summarized in Table S1.

Table S1. The best-fit parameters to the broad Lorentzian peak empirical model for GA solution at pH = 7.[6]

C_{GA} [wt%]	q_0 [A^{-1}] ± 0.0001	Inter-aggregate Distance [nm] ± 0.1	ζ [nm]	*m* ± 0.01
1	0.0165	38.1	1.5 ± 0.2	1.48
2	0.0213	29.5	1.5 ± 0.2	1.25
3	0.0239	26.3	1.2 ± 0.1	1.28
~~5~~	0.0280	22.4	0.8 ± 0.1	1.31

2.2. Phase diagram of SCNCs in water

Figure S2 presents the macroscopic and microscopic behavior of SCNCs suspensions in water. SCNCs suspensions are electrostatically stabilized in water. At low SCNC concentrations, the suspensions are optically isotropic. Above a critical concentration c^*, the suspensions undergo liquid-liquid phase separation to an upper isotropic phase and a lower birefringent liquid crystalline phase. At higher concentrations the volume fraction of the lower non-isotropic phase increases monotonically up to a second critical concentration c^{**}, where the suspension is fully non-isotropic (Figure S2A). POM images reveal that above c^*, the lower phase is chiral nematic (Figure S2C).

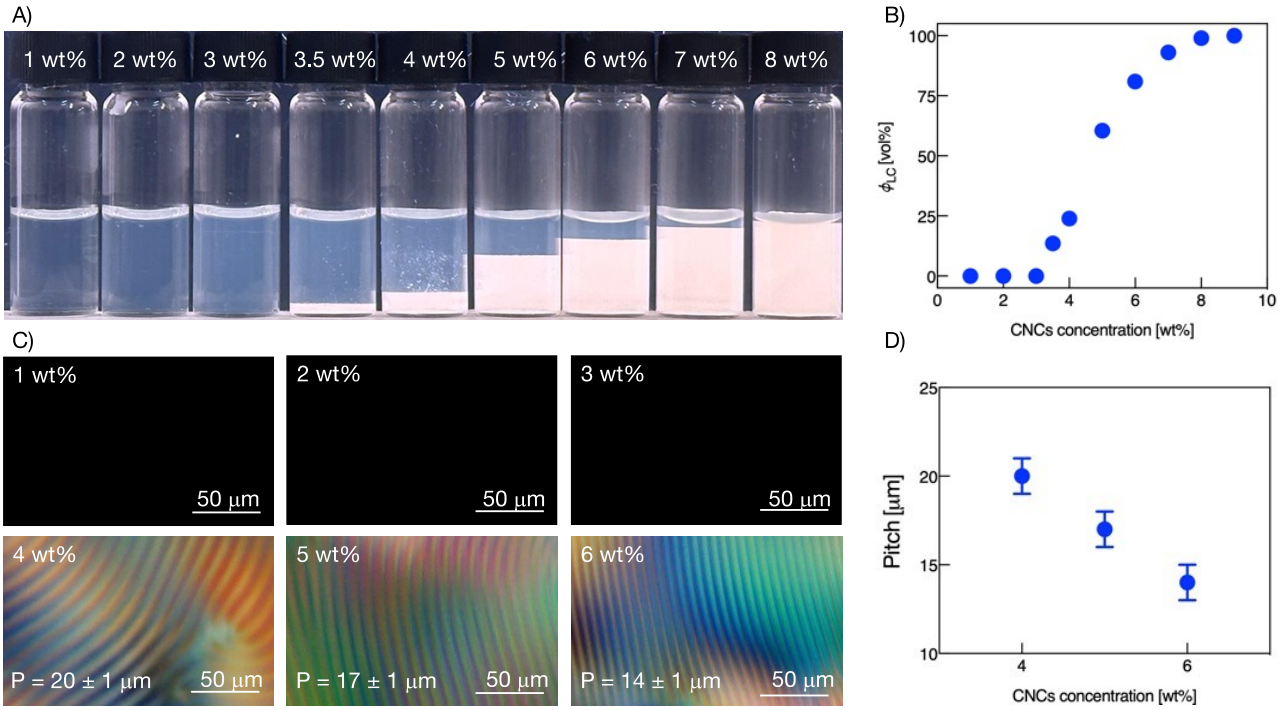

Figure S2. A) Images of vials containing SCNCs suspensions in water at various concentrations, taken between crossed polarizers. The images were taken after two weeks of incubation at room temperature. **B)** Volume fraction of the cholesteric phase (ϕ_{LC}) as a function of SCNCs concentration. C) POM images at C< C* (1-3wt%), and C> C* (4-6 wt%) of the LC phase. **D)** *T*he cholesteric pitch as a function of SCNCs concentration. The pitch was calculated by measuring the distance between the extinction lines ("fingerprint pattern").

The interparticle distance characteristic of SCNCs suspensions in water was investigated using SAXS (Figure S3). The scattering patterns of the aqueous suspensions show the expected behavior.[9–11] 1D SAXS patterns show a peak, q_0, at low q-values and a shoulder at mid-q values q_1, with a q_1/q_0 =2, indicating lamellar symmetry.[12] Higher q-values are measured as the SCNCs concentration is increased, indicating that d_0, calculated from Bragg's law ($d_0 = 2\pi/q_0$), decreases with SCNC concentration. Note that the q_1 and q_0 values were calculated by fitting a Gaussian function to the relevant peaks in Lorentz-corrected intensities plots. d_0 scales with SCNCs concentration (Figure S3 B) as a power law of $d_0 \sim c^{-x}$ *with* $x = 1/3$ *at* low SCNC concentrations, here,1-3 wt%. At the semi-

dilute regime ($C > C^*$, here $C > 3.5$ wt%) d_0 is proportional to $c^{-1/2}$ typical to rods-like particles of nematic ordering.[13] The interparticle distances between SCNC particles were also investigated by cryo-TEM. The TEM images were analyzed using ImageJ software. At least ten TEM images were analyzed, and at least 30 measurements were performed in each image. Table S2 summarizes the data obtained from SAXS and cryo-TEM experiments.

Table S2. SAXS and cryo-TEM data: The position of the peak, shoulder, q_1/q_0 ratio, d_0 obtained from SAXS, and d_0 from cryo-TEM images.

c_{CNCs} [wt%]	c_{GA} [wt%]	q_0 [A^{-1}]	q_1 [A^{-1}]	q_1/q_0	d_0 SAXS [nm]	d_0 Cryo-TEM [nm]
1	-	0.010	0.0182	1.8	63 ± 19	60 ± 19
	1	0.020	-	-	32 ± 3	-
	2	0.025	-	-	25 ± 4	-
	3	0.028	-	-	22 ± 13	22 ± 6
	4	0.032	-	-	20 ± 4	-
2	-	0.011	0.020	1.9	59 ± 17	54 ± 11
	0.5	0.016	0.029	1.9	40 ± 16	-
	1	0.020	0.034	1.8	32 ± 4	24 ± 2
	1.5	0.022	0.043	1.9	28 ± 3	20 ± 3
	2	0.026	0.054	2.1	24 ± 3	-
	3	0.029	0.060	2.0	21 ± 3	22 ± 5

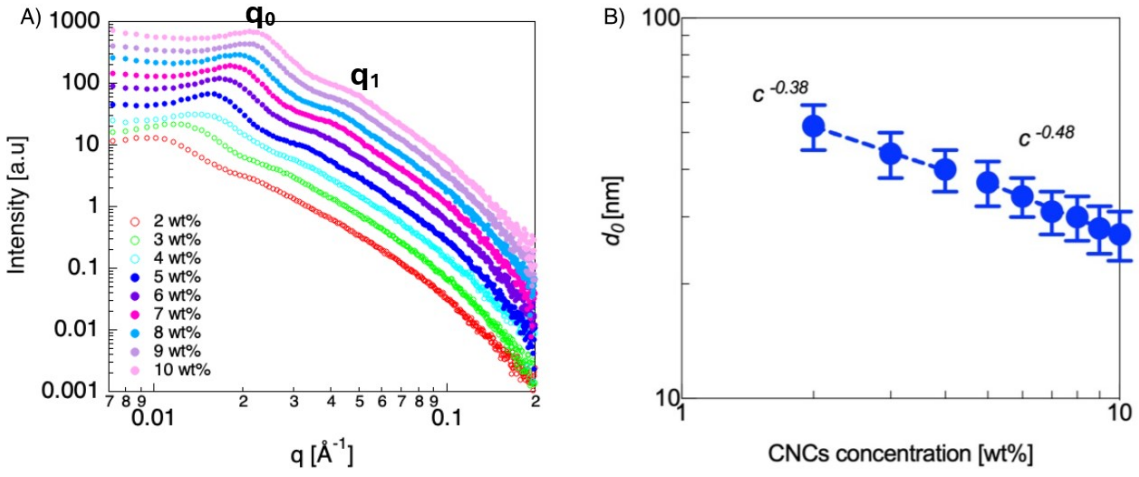

Figure S3. A) 1D SAXS curves obtained from the upper (empty symbols) and Lower phases (filled symbols) of SCNCs suspensions in water. The curves are shifted for better visualization. **B)** The interparticle distance, d_0, as a function of SCNCs concentration.

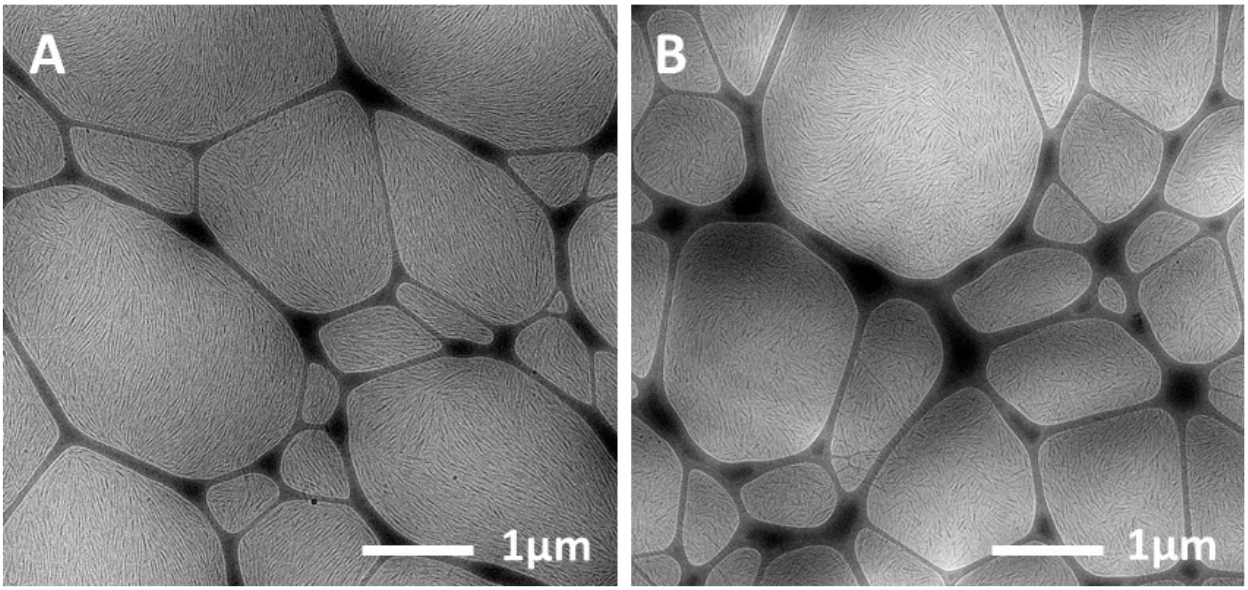

Figure S4. Cryo-TEM low magnification images of 4 wt% suspensions of SCNCS in water. **A)** The N* (lower) phase, **B)** The isotropic (upper) phase.

2.3. SCNCs-GA interactions

Non-adsorption

The effect of GA on the zeta potential of suspended SCNCs rods was characterized *via* zeta potential measurements. The measurements were carried out using the Zetasizer Nano ZS (Malvern Instruments Ltd). The zeta potential was calculated from the electrophoretic mobility following the Henry equation with Smoluchowski approximation:

$$U_E = \frac{2\varepsilon_r \zeta}{3\eta} f(\kappa a) \quad \text{(S1)}$$

Where U_E, ε, ζ, κ, η are the electrophoretic mobility, the dielectric constant of the media, zeta potential, the inverse Debye length, and the viscosity of the media, respectively. For aqueous solutions, the value of $f(\kappa a)$ is 1.5, corresponding to the Smoluchowski approximation.

0.1 wt% SCNCs suspensions in water and 0.01, 0.025, and 0.05 wt% GA solutions were measured. It was found that the Zeta potential of SCNCs in water, is ~ -52 ± 4 mV and is not significantly modified in the presence of GA.

Isothermal titration calorimetry (ITC) experiments, which enable the measurement of the enthalpy of adsorption, were conducted. Titrations of 0.05 and 0.5 wt% GA (syringe) into 0.05 wt% SCNCs in water (cell) at 25 °C were carried out (Figure S5 A, B). The titrations of both 0.05 and 0.5 wt% GA into SCNCs suspensions exhibit small exothermic peaks typical for dilution of GA. For comparison, we present (Figure S5 C, D) titration experiments of 2 wt% PEO (Figure S5 C), a polymer that does not adsorb onto CNCs,[2] and 2 wt% F127, a polymer that adsorbs onto CNCs.[10,11] The results of the zeta potential measurements, along with the ITC experiments indicate that GA does not adsorb onto the SCNCs under the experimental conditions.

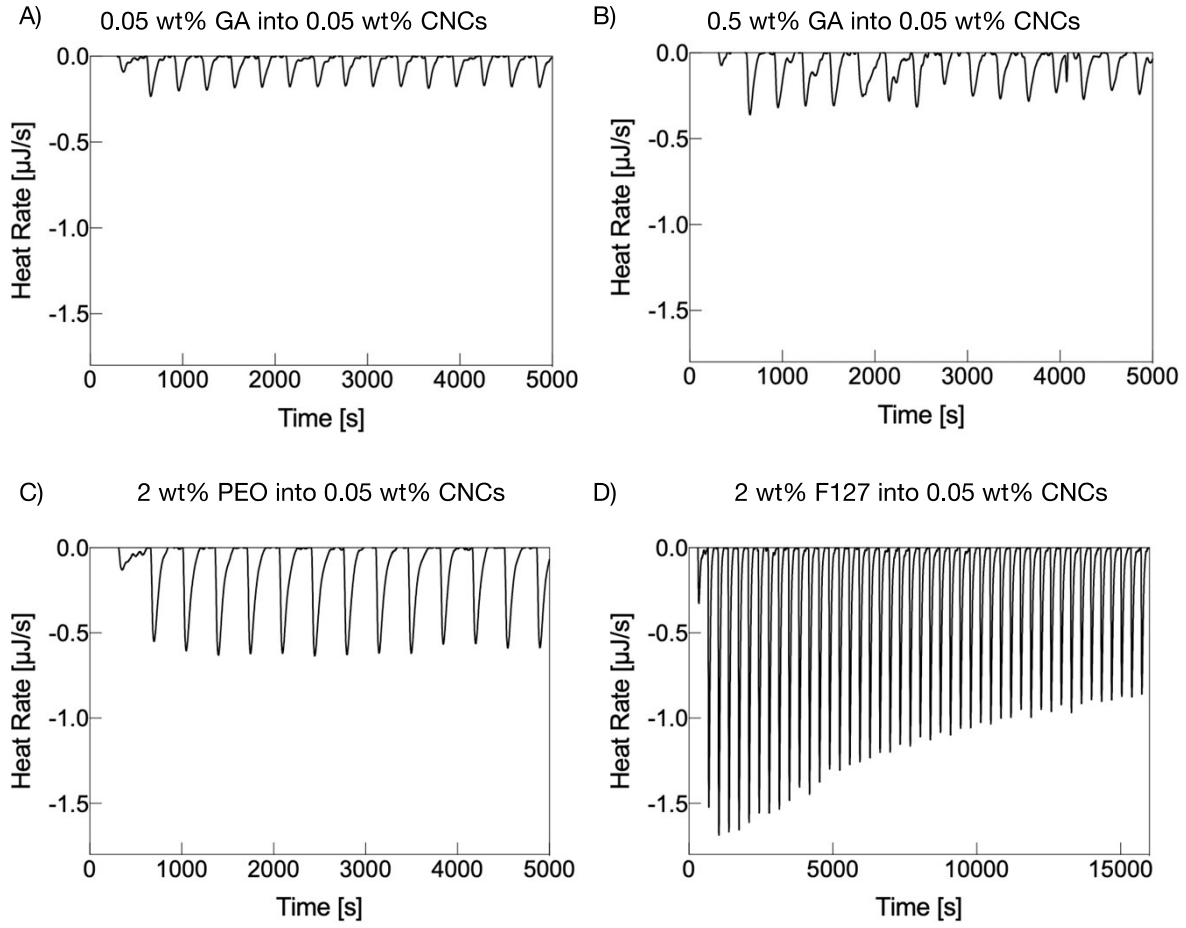

Figure S5. ITC titration curves obtained from titrating **(A)** 0.05 wt%, **(B)** 0.5 wt% GA, and **(C)** 2 wt% PEO, and **(D)** 2 wt% F127 into 0.05 wt% SCNCs at 25 °C.

Modification of the interparticle distance

SAXS and cryo-TEM measurements were used to characterize the effect of solvated GA on the inter-particle distance and self-assembly of SCNCs. Table S3 summarizes the data obtained from SAXS and cryo-TEM experiments in GA solutions. Figures S6 and S7 present SAXS patterns obtained from 1 and 2 wt% CNCs suspensions in GA solutions. The 2D patterns (Figure S7) are isotropic, and similar in water and GA solutions. While suspensions of 1 wt% SCNCs in 1-4 wt% GA solution were found to be fully isotropic and macroscopic phase separation was not detected, 2 wt% SCNCs suspensions in GA solutions exhibit macroscopic phase separation of SCNCs into optically isotropic phase (upper) and a cholesteric phase (lower) from $C_{GA} \geq 1$ wt%.

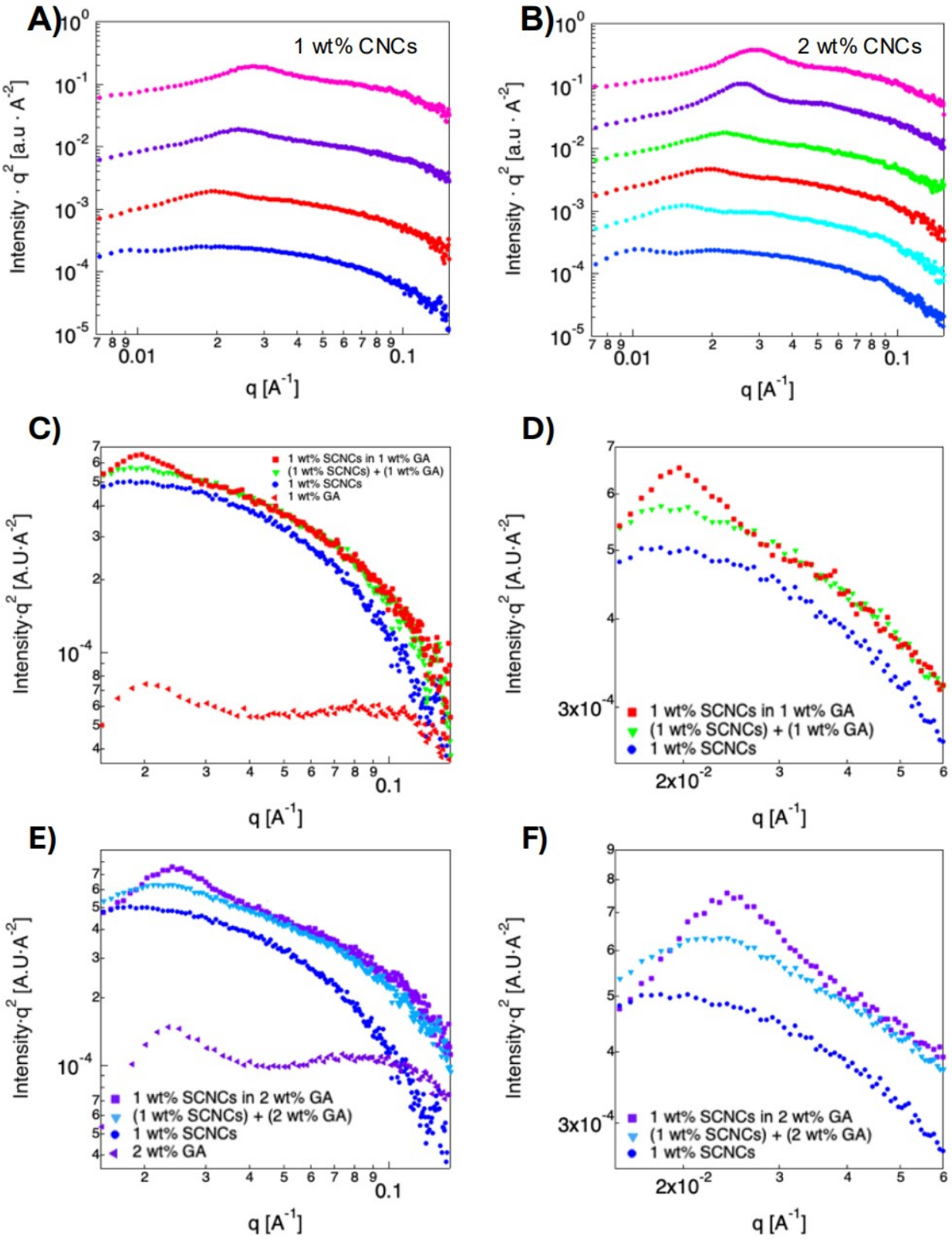

Figure S6. Lorentz-corrected intensities ($I \times q^2$ vs. q) plots of **A)** 1, and **B)** 2 wt% SCNCs suspensions in GA solutions. Color code: ● water, ● 0.5 wt% GA, ● 1 wt% GA, ● 1.5 wt% GA, ● 2 wt% GA, ● 3 wt% GA. The curves are shifted for better visualization. Lorentz-corrected intensities plot representation of the superposition analysis presented in Figure 4 of the main text: 1 wt% SCNCs in 1 wt% GA **C)** the full q-regions, and **D)** zoom-in on the low q-region. 1 wt% SCNCs in 2 wt% GA **E)** the full q-regions, and **F)** zoom in on the low q-region.

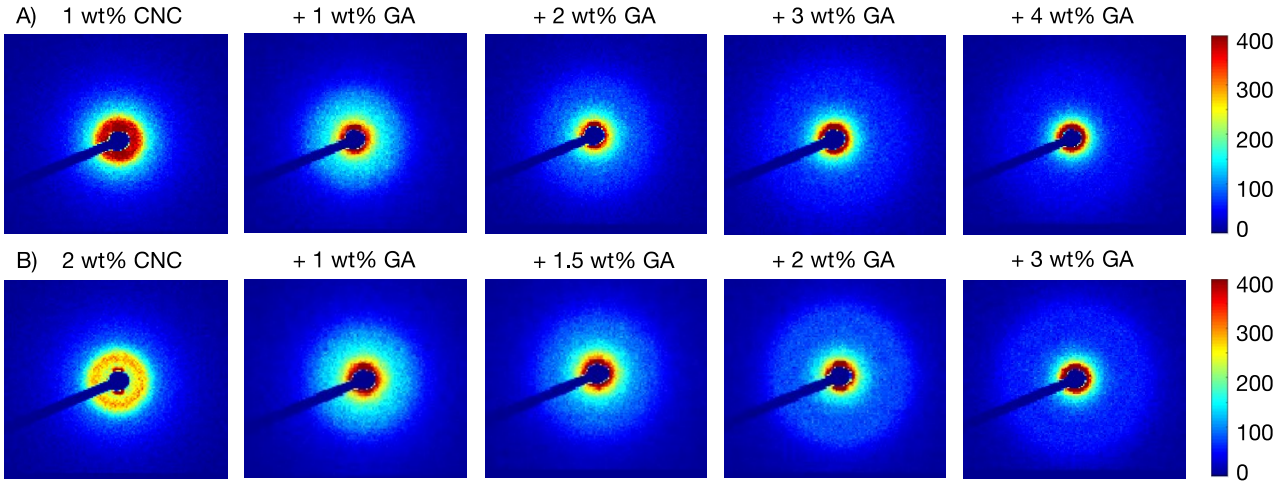

Figure S7. 2D SAXS patterns obtained from **A)** 1 and **B)** 2 wt% SCNCs suspensions in water and solutions of GA.

Table S3. The average interparticle distances d_0 that were measured in SAXS and cryo-TEM images.

C_{SCNCs} [wt%]	c_{GA} [wt%]	q_0 [A^{-1}]	q_1 [A^{-1}]	q_1/q_0	d_0 SAXS [nm]	d_0 Cryo-TEM [nm]
3	-	0.014	0.028	2.0	44 ± 6	46 ± 8
	0.5	0.018	0.036	1.9	34 ± 4	-
	1	0.022	0.043	2.0	29 ± 5	22 ± 5
	1.5	0.025	0.049	2.0	25 ± 4	-
	2	0.027	0.053	2.0	23 ± 3	-
	3	0.031	0.061	1.9	20 ± 3	-

As mentioned above, in GA solutions, the threshold concentrations of the bi-phasic regime (*I-N** coexistence) are shifted from 3.5 wt% SCNCs (in water, Figure S2) to below 1.5 wt% SCNCs. Thus, 3 wt% SCNCs suspensions that contain 1 wt% GA show a macroscopic isotropic (upper) phase and nematic (lower) phase.

2D SAXS patterns of these suspensions (Figure S8 A, D) clearly show that the upper phase is isotropic while the lower phase is not. The 1D scattering curves (Figure S8 B, E) exhibit the typical structure of SCNCs phases, with a nematic character but a small inter-particle distance (below 20 nm).

POM images (Figure S8 C, F) reveal the presence of cholesteric tactoids in the upper phase (Figure S8C) that are similar to those observed in SCNCs suspensions at concentrations above C_w*.

The birefringent (lower) phase exhibits the typical fingerprint pattern characteristic of the SCNCs *N** phase (Figure S8F).

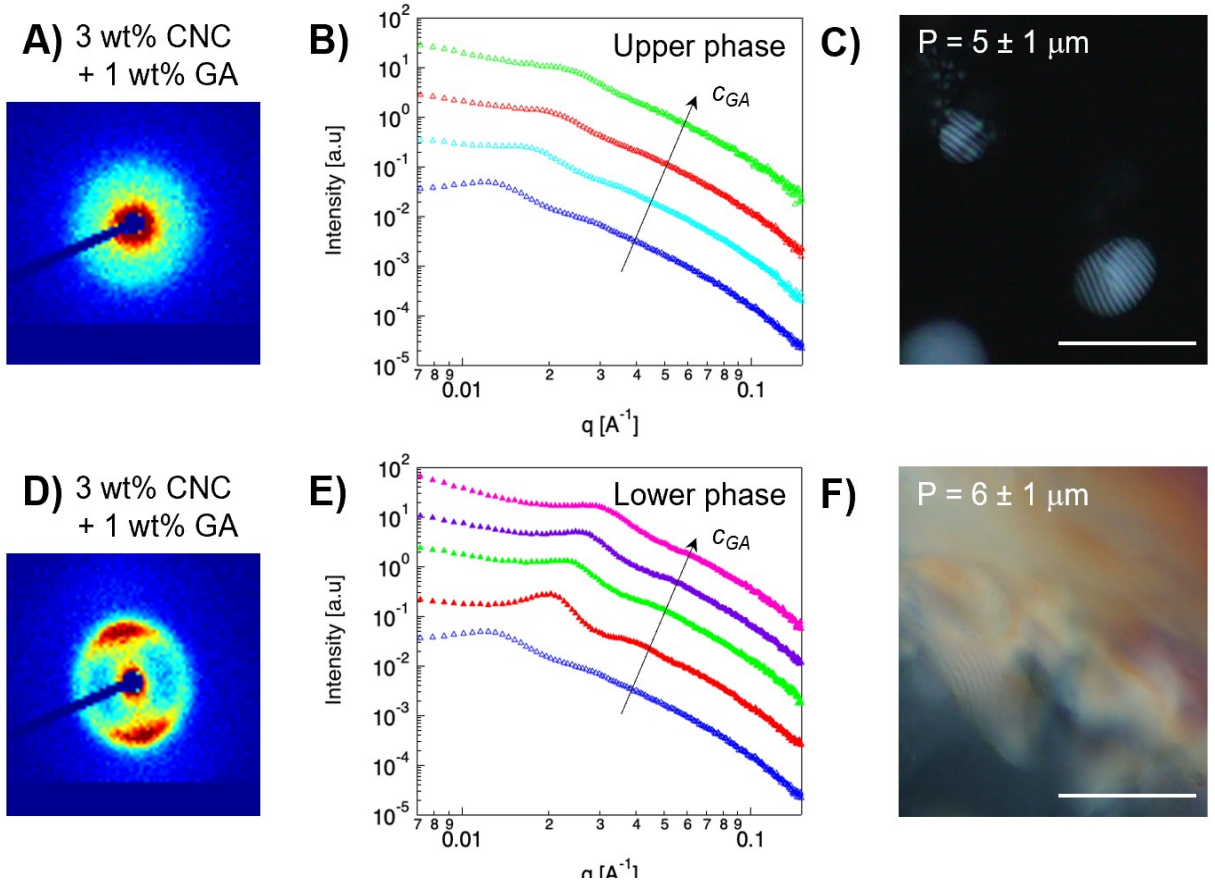

Figure S8. The isotropic phase of 3 wt% SCNCs suspensions in GA solution: **A)** 2D SAXS pattern obtained from 3 wt% SCNCs in 1 wt% GA. **B)** 1D SAXS curves of 3 wt% SCNCs in water (△), 0.5 wt% GA (△), 1 wt% GA (△), 1.5 wt% GA (△). The curves are shifted for better visualization. **C)** POM image of 3 wt% SCNCs in 1 wt% GA. The non-isotropic phase of 3 wt% SCNCs suspensions in GA solution: **D)** 2D SAXS pattern obtained from 3 wt% SCNCs in 1 wt% GA. **E)** 1D SAXS curves of 3 wt% SCNCs in water (▲),1 wt% GA (▲), 1.5 wt% GA (▲), 2 wt% GA (▲), 3 wt% GA (▲). The curves are shifted for better visualization. **F)** POM image of 3 wt% SCNCs in 1 wt% GA.

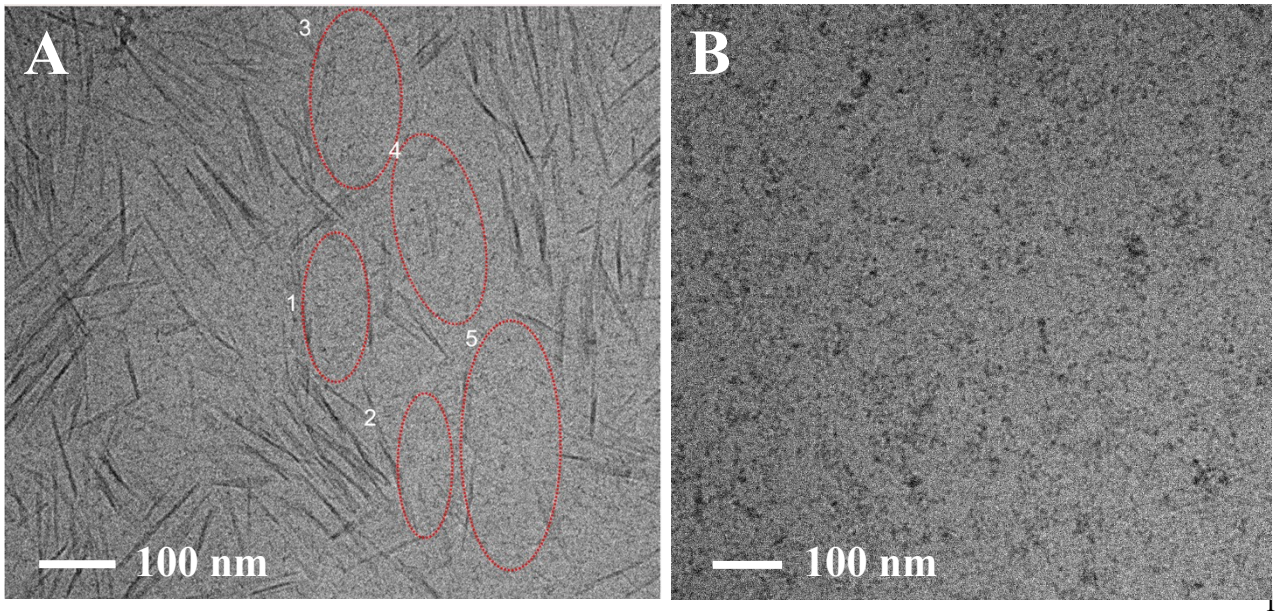

Figure S9. A) A cryo-TEM image of 2wt% SCNCs in solution of 1 wt% GA**.** The calculated typical inter-SCNCs distance is 19 nm. Standard deviation= 2 nm. B) TEM image of solution of 1wt% GA stained with 2 wt% Uranyl-acetate salt used for enhancing the contrast (since the heavy Uranyl ions scatter electrons much better than the low-weight organic components of the GA polymer).

Table S4. Analysis (by ImageJ software) of the features in the cryo-TEM image. Marked in red: SCNCs-poor & GA-Rich areas.

GA –rich phase (marked droplets)			
No.	Length [nm]	Width [nm]	No.
1	207	91	15236.30
2	201	112	18504.52
3	293	136	33474.06
4	343	138	38647.34
5	348	138	38487.71

REFERENCES

(1) Edgar, C. D.; Gray, D. G. Influence of Dextran on the Phase Behavior of Suspensions of Cellulose Nanocrystals. *Macromolecules* **2002**, *35* (19), 7400–7406. https://doi.org/10.1021/MA0204195/ASSET/IMAGES/LARGE/MA0204195F00008.

(2) Sun, Q.; Lutz-Bueno, V.; Zhou, J.; Yuan, Y.; Fischer, P. Polymer Induced Liquid Crystal Phase Behavior of Cellulose Nanocrystal Dispersions. *Nanoscale Adv* **2022**, *4* (22). https://doi.org/10.1039/d2na00303a.

(3) Oguzlu, H.; Dobyrden, I.; Liu, X.; Bhaduri, S.; Claesson, P. M.; Boluk, Y. Polymer Induced Gelation of Aqueous Suspensions of Cellulose Nanocrystals. *Langmuir* **2021**, *37* (10), 3015–3024. https://doi.org/10.1021/ACS.LANGMUIR.0C02336/SUPPL_FILE/LA0C02336_SI_001.

(4) Oguzlu, H.; Boluk, Y. Interactions between Cellulose Nanocrystals and Anionic and Neutral Polymers in Aqueous Solutions. *Cellulose* **2017**, *24* (1), 131–146. https://doi.org/10.1007/S10570-016-1096-6/METRICS.

(5) Bardet, R.; Belgacem, N.; Bras, J. Flexibility and Color Monitoring of Cellulose Nanocrystal Iridescent Solid Films Using Anionic or Neutral Polymers. *ACS Appl Mater Interfaces* **2015**, *7* (7), 4010–4018. https://doi.org/10.1021/AM506786T/SUPPL_FILE/AM506786T_SI_001.

(6) Horkay, F.; Hammouda, B. Small-Angle Neutron Scattering from Typical Synthetic and Biopolymer Solutions. *Colloid and Polymer Science*. 2008. https://doi.org/10.1007/s00396-008-1849-3.

(7) Nishida, K.; Kaji, K.; Kanaya, T.; Shibano, T. Added Salt Effect on the Intermolecular Correlation in Flexible Polyelectrolyte Solutions: Small-Angle Scattering Study. *Macromolecules* **2002**, *35* (10). https://doi.org/10.1021/ma010572j.

(8) Dror, Y.; Cohen, Y.; Yerushalmi-Rozen, R. Structure of Gum Arabic in Aqueous Solution. *J Polym Sci B Polym Phys* **2006**, *44* (22). https://doi.org/10.1002/polb.20970.

(9) Schütz, C.; Agthe, M.; Fall, A. B.; Gordeyeva, K.; Guccini, V.; Salajková, M.; Plivelic, T. S.; Lagerwall, J. P. F.; Salazar-Alvarez, G.; Bergström, L. Rod Packing in Chiral Nematic Cellulose Nanocrystal Dispersions Studied by Small-Angle X-Ray Scattering and Laser Diffraction. *Langmuir* **2015**, *31* (23). https://doi.org/10.1021/acs.langmuir.5b00924.

(10) Attia, D.; Yekymov, E.; Shmidov, Y.; Levi-kalisman, Y.; Mendelson, O.; Bitton, R.; Yerushalmi-rozen, R. Surfactant-mediated Co-existence of Single-walled Carbon Nanotube Networks and Cellulose Nanocrystal Mesophases. *Nanomaterials* **2021**, *11* (11), 3059. https://doi.org/10.3390/NANO11113059/S1.

(11) Cohen, N.; Attia, D.; Levi-Kalisman, Y.; Bitton, R.; Yerushalmi-Rozen, R. Emergent Hybrid Mesophases in Ternary Mixtures of Cellulose Nanocrystals - Pluronic Micelles-Water. *Polym Adv Technol* **2022**, *33* (11), 3800–3809. https://doi.org/10.1002/PAT.5647.

(12) Alexandridis, P.; Olsson, U.; Lindman, B. A Record Nine Different Phases (Four Cubic, Two Hexagonal, and One Lamellar Lyotropic Liquid Crystalline and Two Micellar Solutions) in a Ternary Isothermal System of an Amphiphilic Block Copolymer and Selective Solvents (Water and Oil). *Langmuir* **1998**, *14* (10). https://doi.org/10.1021/la971117c.

(13) Munier, P.; Di, A.; Hadi, S. E.; Kapuscinski, M.; Segad, M.; Bergström, L. Assembly of Cellulose Nanocrystals and Clay Nanoplatelets Studied by Time-Resolved X-Ray Scattering. *Soft Matter* **2021**, *17* (23), 5747–5755. https://doi.org/10.1039/D1SM00251A.